Force measurements on plasma actuators using phase-locked particle image velocimetry

R. Pimentel
A. Lahouti
DRDC – Valcartier Research Centre

P. Lavoie
University of Toronto

Defence Research and Development Canada

Scientific Report
DRDC-RDDC-2015-R071
May 2015

Force measurements on plasma actuators using phase-locked particle image velocimetry

R. Pimentel
A. Lahouti
DRDC – Valcartier Research Centre

P. Lavoie
University of Toronto

Defence Research and Development Canada

Scientific Report
DRDC-RDDC-2015-R071
May 2015

Abstract

Phase-locked Particle Image Velocimetry (PIV) has been used to investigate the time-dependent behaviour of a Dielectric Barrier Discharge (DBD) plasma actuator, excited by a sine-wave signal with peak-to-peak amplitudes between 7.2 kV and 10 kV, and frequencies of 2.5 kHz and 4 kHz. Measurements were initially carried out in a 31.5 mm x 15 mm domain, resulting in a spatial resolution of 0.1072 mm, in 12 phase intervals throughout the excitation cycle. In order to improve the spatial and temporal resolution, additional measurements were carried out for a subset of the excitation parameters in an 8.1 mm x 6.1 mm domain, resulting in a spatial resolution of 0.0276 mm in 24 phase intervals. Momentum balance in a control volume surrounding the actuator has been used to estimate the body force based on the results of the PIV measurements. The results indicate that the maximum induced velocity and body force occur during the negative half-cycle of the excitation signal, with a phase lag relative to the excitation signal that grows when excitation voltage or frequency is increased. A smaller, secondary peak is observed in the induced body force, occurring during the positive half-cycle of the excitation signal. The results suggest that this peak is due to formation of a secondary high-velocity region due to local discharges near the grounded electrode. Two methods have been used to determine the shear force, resulting up to 25% variability in the estimated body force. Considering this variability, direct force measurements have been carried out using a precise balance to validate the results of the PIV-based control volume approach. The difference observed in certain conditions between the estimated body forces and those measured directly highlight the need for further improving the methodology for body force prediction based on PIV measurements.

Significance to defence and security

Requirements of high-speed vehicles for military and civilian applications have driven interest on novel flow control strategies; however, traditional techniques are complex and expensive. A promising new flow control technique is the DBD actuator. The potential of these actuators as flow control devices has been demonstrated in the control of laminar-to-turbulent transition of boundary layers, shock-boundary layer interactions, and flow field modification over airframes to modify stability and control characteristics. The flow control mechanism of these Electrohydrodynamic (EHD) devices is through a generated body force field caused by the actuator, which couples with the momentum of the external flow. Potential benefits of EHD devices are very large and span from several military and civilian applications and this technology has prompted significant interest and investment worldwide. Its potential use is continuously extending and includes several fields of interest to DND, such as propulsion and heat transfer minimization. Nevertheless, the complex physical phenomena associated with these actuators is not fully understood, and most research is limited to laboratory environments aimed at understanding key parameters affecting performance as well as physical operating principles of these devices. There remain several issues to overcome before this technology can be integrated into practical applications. For instance, the effects of operating conditions on EHD actuator performance, electrical power requirements and suitability to high-speed regimes are some of the parameters that must be addressed before incorporating such devices into practical systems.

Résumé

La technique vitesse par image de particule (PIV) à verrouillage de phase a été utilisée pour étudier le comportement temporal d'un actionneur plasma de décharge à barrière diélectrique (DBD) excité par un signal sinusoïdal avec des amplitudes crête-à-crête entre 7,2 kV et 10 kV, et les fréquences de 2,5 kHz et 4 kHz. Les mesures ont été réalisées dans un premier temps sur un domaine de 31,5 mm x 15 mm, ce qui entraîne une résolution spatiale de 0,1072 mm, à 12 intervalles de phase pendant tout le cycle d'excitation. Afin d'améliorer la résolution spatiale et temporelle, des mesures supplémentaires ont été effectuées pour un sous-ensemble des paramètres d'excitation dans un domaine de 8,1 mm x 6,1 mm, ce qui entraîne une résolution spatiale de 0,0276 mm, à 24 intervalles de phase. Le bilan de la quantité du mouvement dans un volume de contrôle entourant l'actionneur a été utilisé pour estimer la force de corps basé sur les résultats des mesures par PIV. Les résultats indiquent que la vitesse et la force maximales se produisent pendant le demi-cycle négatif du signal d'excitation, avec un retard de phase par rapport au signal d'excitation qui agrandit lorsque la tension ou la fréquence d'excitation augmente. Un petit pic secondaire est observé dans la force induite se produisant pendant le demi-cycle positif du signal d'excitation. Les résultats suggèrent que ce pic est dû à la formation d'une région secondaire de grande vitesse en raison de décharges locales à la proximité de l'électrode encapsulé. Deux méthodes ont été utilisées pour déterminer la force de cisaillement, ce qui entraîne jusqu'à 25% de variation sur la force de corps estimée. Compte tenu de cette variabilité, des mesures directes de force ont été effectuées en utilisant une balance de précision pour valider les résultats de l'approche basée sur la technique PIV. La différence observée dans certaines conditions entre les forces corporelles estimées et celles mesurées directement mettre en évidence la nécessité de s'améliorer la méthodologie pour la prédiction de la force de corps obtenues par la technique PIV.

Importance pour la défense et la sécurité

Les exigences des véhicules à grande vitesse pour des applications militaires et civiles ont entraîné un intérêt sur les technologies innovatrices pour le contrôle d'écoulement. Différentes stratégies pour le contrôle d'écoulement à haute vitesse ont été utilisées; Cependant, les technologies traditionnelles pour le contrôle d'écoulement sont complexes et coûteuses. Une nouvelle technologie prometteuse est celle des actionneurs plasma à décharge à barrière diélectrique. Le potentiel de ces actionneurs comme dispositifs de contrôle d'écoulement a été démontré lors du contrôle de la transition laminaire-turbulente de la couche limite, des interactions ondes de choc-couche limite, ainsi que lors de la modification du champ d'écoulement autour des aéronefs afin de modifier leurs caractéristiques de stabilité et de contrôle. Le mécanisme de contrôle d'écoulement de ces dispositifs électro-hydrodynamique est par une force de volume générée par l'actionneur, laquelle se couple avec la quantité de mouvement de l'écoulement externe. Les avantages potentiels de ces dispositifs sont très grands et couvrent un vaste champ d'applications militaires et civiles. Cette technologie a suscité beaucoup d'intérêt et d'investissements partout dans le monde. Le nombre d'applications potentielles de cette technologie s'accroît continuellement et comprend plusieurs champs d'intérêt pour le MDN, comme la propulsion et la minimisation de transfert de chaleur. Toutefois, les phénomènes

physiques complexes associés à ces actionneurs ne sont pas entièrement compris et la plupart des recherches sont limitées à des conditions de laboratoire visant à comprendre les paramètres clés qui influencent la performance ainsi que les principes de fonctionnement de ces dispositifs. Il reste plusieurs questions à résoudre avant que cette technologie puisse être intégrée dans des applications pratiques.

This page intentionally left blank.

Table of contents

List of figures

This page intentionally left blank.

1 Introduction

Dielectric Barrier Discharge (DBD) plasma actuators are gaining increasing acceptance as flow control devices, due to their unique features including independence from external sources of flow, and relatively low geometric profile, which makes them relatively easy to implement. The growing range of successful application of plasma actuators for flow control includes control of transition of a laminar boundary layer [1] , control of flow separation on an airfoil [2], and control of bluff body wakes [3]. Many of these applications involve unsteady flow phenomena of various time scales, which require the use of active flow control for more effective interaction with the flow. One of the important aspects in active flow control is the time-dependent behaviour of the actuator, and in particular its temporal response to actuator commands. This characteristic becomes particularly significant when the dominant time scales of the flow phenomenon and the temporal response of the actuator are of the same order of magnitude. The study of the time-dependent behaviour of plasma actuators also provides a better understanding of their flow physics, which are closely related to the characteristics of the unsteady excitation signal. Improving the current knowledge in the two above-mentioned areas has been the primary motivation of this study.

Various measurement techniques have been used in the past to investigate the time-dependent characteristics of the flow induced by plasma actuators. Boucinha et al. [4] have used Laser Doppler Velocimetry (LDV) to measure the induced velocity at a number of significant locations near a DBD plasma actuator. In their experiments, the velocity generated by exciting the actuator at a frequency of 1 kHz was measured at an average sampling rate of 4 kHz. While this sampling rate made it possible to demonstrate that the flow induced by the actuator varied through the excitation cycle, it was not sufficient to produce a high-resolution time-resolved representation of the behaviour of the induced flow. Furthermore, since LDV is a line of sight technique, a large number of separate measurements would be needed to characterize the entire flow field using this technique, making this measurement method particularly susceptible to eventual deterioration of the plasma actuator in long-duration operation [5].

Kotsonis and Ghaemi [6] have used Time-Resolved Particle Image Velocimetry (TR-PIV) to characterize the flow field around DBD plasma actuators excited by various waveforms. In their experiments, the actuator was excited at a frequency of 625 Hz, and the sampling rate was 6 kHz. While the time-dependent behaviour of the actuator was resolved with remarkable temporal resolution in their study, the excitation frequency was much lower than typical values of interest found in most other studies. This highlights the fact that application of this technique in general is limited to lower actuator excitation frequencies, due to limits in the sampling frequency of current TR-PIV systems and the prohibitive cost and technical challenges of very high frequency PIV measurements. As an example, to obtain a similar temporal resolution for a plasma actuator excited at a typical frequency of 5 kHz, a TR-PIV system with an unusually high sampling rate of 50 kHz would be needed.

DBD plasma actuators are usually excited using an Alternating Current (AC) signal. The periodic nature of the excitation signal makes it possible to use it as a triggering source for synchronized, phase-locked measurements. Phase-locked PIV measurement is an accessible and consistent alternative to the above-mentioned time-resolved techniques for characterizing the time-dependent behaviour of flow induced by plasma actuators. One of the earliest examples of

the use of this technique is the study by Kim et al. [7] to investigate the role of elevated levels of oxygen on improvement of the velocity induced during the positive half-cycle of the excitation voltage. This study shows the merit of this technique for measuring the entire flow field at the desired instances through the excitation cycle using a non-time-resolved PIV system, even when the excitation frequency is relatively large. Another example of the utilization of phase-locked PIV measurements to characterize the time-dependent behaviour of plasma actuators is the study by Murphy et al. [8], in which the effect of the amplitude of the excitation voltage on spatial and temporal variations of peak momentum transfer throughout the excitation cycle have been investigated.

The present study extends the scope of the study by Murphy et al. [8] in several directions, while retaining the same physical configuration and geometry for the plasma actuator, to facilitate comparison with previous findings. The focus of the present study is to characterize the phase-dependent behaviour of the maximum induced velocity and its location, as well as the induced body force through the excitation cycle, using phase-locked PIV measurements with improved temporal and spatial resolution. Specifically, the number of phase intervals at which PIV measurements are carried out through the excitation cycle, is increased from 8 to 12, and in selected cases to 24, with concentration in the vicinity of the phase angles associated with the maximums of the induced velocity and body force. Also, the spatial resolution is improved to less than 0.03 mm in selected cases, using a catadioptric microscopic lens.

Furthermore, in this study the measurements were carried out at two excitation frequencies, thus making it possible to investigate the effects of excitation frequency on the above-mentioned phase-dependent characteristics. Finally, the present study also includes a detailed investigation of the wall shear stress as a significant contributor to the induced body force. This investigation includes the effect of various estimation methods on the body force component resulting from wall shear stress, and an attempt to validate the body force estimation methods based on PIV measurements against direct body force measurements using a force balance.

The Scientific Report is structured as follows. In Section 2, the details of the experimental apparatus and procedures, including the plasma actuator, the electronics used for excitation and monitoring, PIV and force measurement equipment are described. In Section 3, the results of the flow field and force measurements are presented and analyzed. These results include the phase-dependent behaviour of the induced velocity, the phase-dependent behaviour of the estimated body force and the role of wall shear stress in body force estimation, and direct force measurements. The principal findings of the study are summarized in Section 0. Based on these findings, recommendations have been made to improve the results and further expand the scope of the study.

2 Experimental setup

The plasma actuator used in the present experiments comprised of two 80 μm thick copper electrodes, separated by four layers of Kapton® tape as dielectric. Each layer of Kapton® tape was 0.089 mm thick, bringing the total dielectric thickness to 0.356 mm. A plate made of Poly(methyl methacrylate (PMMA) or Acrylic with a thickness of 3 mm was used as substrate, to support the electrodes and the dielectric layer. The widths of the exposed and grounded electrodes were 6.35 mm and 19.05 mm, respectively, and the span of both electrodes was 150 mm. No gap existed between the adjacent edges of the exposed and the grounded electrodes.

Throughout all experiments, the actuator was placed in a cubic chamber with a side length of 0.68 m, made of transparent PMMA, to isolate it from ambient disturbances. During PIV experiments, the actuator was supported by a 4 degree of freedom (3 translational and 1 rotational degree of freedom) stage, which facilitated the precise positioning of the actuator within the field of view of the camera, as presented in Figure 1.

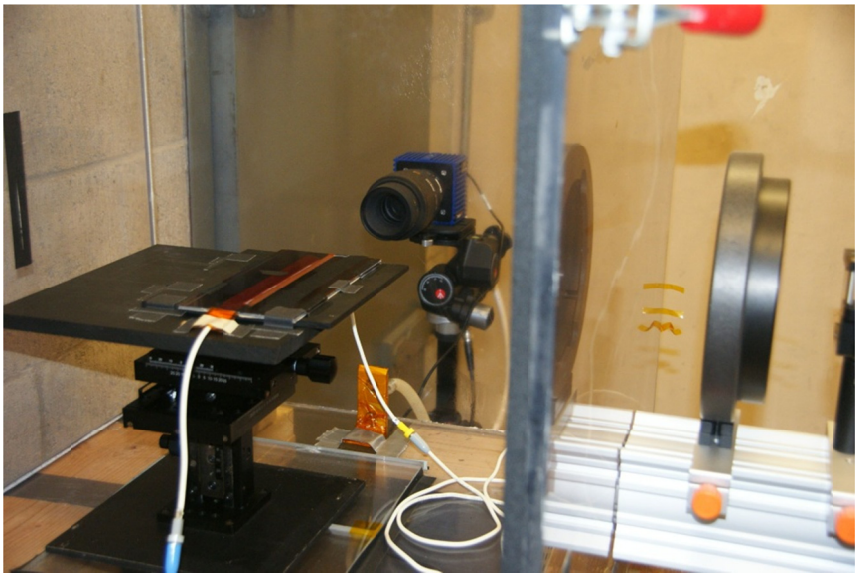

Figure 1: *The plasma actuator, mounted on the 4 degree of freedom stage for positioning during PIV measurements.*

During direct force balance measurements, the actuator was placed on the force balance via a rigid support assembly, shown in Figure 2.

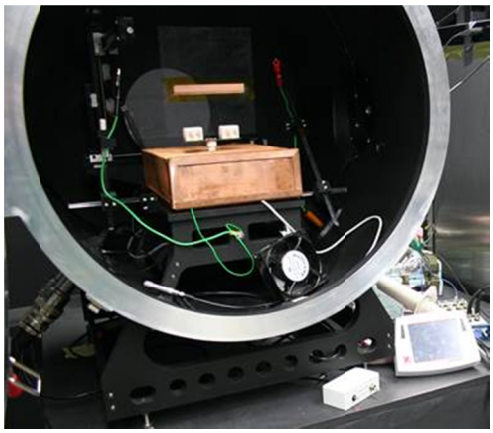

Figure 2: *The direct force measurement setup including the plasma actuator, the force balance (inside the Faraday cage), the 44 American wire gauge (AWG) wire electrical connection, and the high voltage probe.*

The plasma actuator was excited by a sine-wave signal, which was generated by an Agilent 33210A function generator (Figure 3), and amplified by a ratio of 2000:1 using a Trek Model 20/20C amplifier (Figure 5). The accuracy of the excitation signal was ±0.05 Hz at 2.5 kHz and ±0.08 Hz at 4.0 kHz.

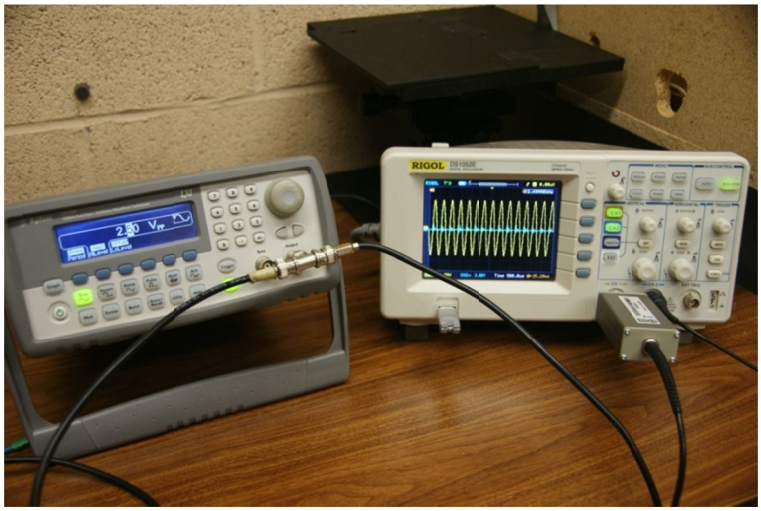

Figure 3: *The function generator used to generate the excitation signal for the plasma actuator and the triggering signal for the PIV system (left) and the digital oscilloscope (right).*

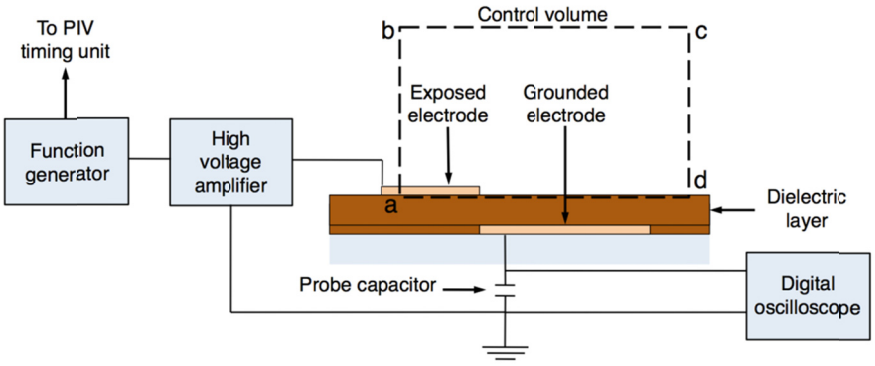

Figure 4: *Schematic view of the plasma actuator setup showing the position of the control volume for body force estimation relative to the actuator.*

Figure 5: *The PIV measurement setup, and the high voltage amplifier.*

During each experiment, the electric power consumption of the plasma actuator was measured using the probe capacitance method described by Kriegseis et al. [9]. In accordance with the methodology described in [9], the capacitance of the probe capacitor should be three orders of magnitude larger than the cold capacitance of the plasma actuator. The excitation voltage of the plasma actuator and the voltage across the probe capacitor were measured and recorded using a

Rigol 1052E digital oscilloscope, simultaneous with the PIV and force balance measurements. The voltages were recorded simultaneously with each PIV and force balance experiment during 20 ms, which spanned 50 and 80 cycles at the excitation frequencies of 2.5 kHz and 4.0 kHz, respectively. A schematic diagram of the electronic components of the plasma actuator setup is shown in Figure 4.

PIV technique was used to measure the velocity field around the actuator. A LaVision PIV system including an Imager SX-4M (Charge-Coupled Device) camera with a resolution of 2386 x 1776 pixels, and an Evergreen 200 mJ/pulse Nd-YAG laser was utilized (Figure 5). Velocity vector fields were obtained using a cross-correlation scheme in 16 x 16 interrogations windows with 50% overlap, resulting an array of 295 x 222 vectors for each image pair. Phase-locked measurements were carried out using the excitation signal generated by the function generator as an external trigger for the PIV system Programmable Timing Unit (PTU). The phase angle for each set of measurements was specified by adjusting the time delay between the trigger signal and the recording of the image pairs in the PIV system.

PIV measurements were carried out in two different measurement domains. Initially, measurements were carried out using a Sigma 105 mm f/2.8 EX DG macro lens in a domain measuring 31.5 mm in the horizontal (x) direction and 15 mm in the wall-normal (y) direction, with the downstream edge of the exposed electrode ($x = y = 0$) located 8 mm upstream of the centre of the measurement domain. The spatial resolution (spacing between the adjacent vectors) in this domain was 0.1072 mm. In this measurement domain, for each experiment involving a particular combination of excitation parameters, phase-locked measurements were carried out at 12 phase angles at $\pi/4$ rad intervals in the positive half-cycle of the excitation signal, and $\pi/8$ rad intervals, with 300 image pairs for each phase angle. Consequently, to increase the number of phase angles in the phase-locked measurements as described in Section 3.1, a Questar QM-1 catadioptric lens with a 35 mm equivalent focal length of 1700 mm (Figure 6) was used.

Figure 6: *The Questar QM-1 catadioptric microscopic lens, attached to the PIV camera.*

The use of the QM-1 lens reduced the size of the measurement domain to 8.1 mm in the horizontal (x) direction and 6.1 mm in the wall-normal (y) direction, and improved the spatial resolution to 0.0276 mm. To acquire data in an area large enough for application of the control volume method for body force estimation (Section 3.2), measurements using the QM-1 lens were carried out in two side-by-side windows for each combination of phase angle and excitation parameters. The first measurement window extended from 1.66 mm upstream to

6.44 mm downstream of the downstream edge of the exposed electrode ($x = y = 0$). The second measurement window extended from 5.98 mm downstream to 14.09 mm downstream of the downstream edge of the exposed electrode. In these measurement domains, for each experiment involving a particular combination of excitation parameters, phase-locked measurements were carried out at 24 phase angles at $\pi/8$ rad intervals in the positive half-cycle of the excitation signal, and $\pi/16$ rad intervals in the negative half-cycle, with 250 image pairs for each phase angle.

Direct measurements of the force generated by the plasma actuator was carried out using a Ohaus Explorer Ex-324 balance, which had a resolution of 0.0001 g and a linearity less than ±0.0002 g. As shown in Figure 2, the balance was placed in a Faraday cage connected to the electric ground connection of the laboratory, to minimize electromagnetic interference.

Electrical connection between the actuator and the power supply was established using 44 American Wire Gauge (AWG) copper wires with nominal bare diameter of 0.0508 mm, to ensure that the electrical connection does not impose any mechanical constraint on the actuator during force measurements (Figure 2).

3 Results and discussions

3.1 Time dependent behaviour of velocity

An example of the results of phase-locked PIV measurements of the velocity field around the plasma actuator in the 31.5 mm x 15 mm domain described in Section 2 is shown in Figure 7. The figure shows the evolution of the induced velocity magnitude ($|V| = \sqrt{u^2 + v^2}$) throughout the excitation cycle, for an excitation peak-to-peak voltage of 8.8 kV (8.8 kVpp) and an excitation frequency of 4 kHz. It can be observed that a phase lag exists between the maximum of the excitation voltage, which occurs at $\Phi = 0$, and the maximum of the induced velocity, which occurs at $\Phi = 11\pi/8$. The maximum of the induced velocity occurs during the negative half-cycle of the excitation voltage, when the exposed electrode has a negative charge. The phase lag, which is of particular interest in application of plasma actuators for active flow control, can be investigated in more detail by examining the time-dependent behaviour of the maximum induced velocity relative to the excitation signal, for various combinations of excitation parameters.

Figure 8 shows the variation of maximum magnitude of the induced velocity throughout the excitation cycle for three excitation voltages of 7.2 kVpp, 8.8 kVpp, and 10 kVpp, applied at 2.5 kHz (Figure 8a) and 4.0 kHz (Figure 8b). The average values of the induced velocity magnitude are in close agreement with those reported by Murphy et al. [11] for the same plasma actuator. However, the figure indicates that the phase lag between the maximum induced velocity and the excitation voltage is not constant. Figure 9 shows the trend of variation of the phase lag with excitation parameters. It can be observed that the phase lag increases slightly when the actuator is excited with a higher voltage. This effect is more pronounced at the excitation frequency of 4 kHz, where relatively larger values of phase lag are observed.

Another interesting aspect of the time dependent behaviour of the plasma actuator is the location of the maximum induced velocity within the measurement domain. As shown in Figure 10, the location of maximum velocity depends on the phase angle. The figures indicate a general trend in which the location of the maximum induced velocity is closer to the downstream edge of the exposed electrode ($x = y = 0$) during the negative half-cycle of the excitation signal, and farther from it during the positive half cycle. This trend, which is the opposite of the phase-dependent behaviour of the maximum induced velocity (Figure 8) suggests that during the negative-half cycle, when the exposed electrode has a negative charge, the largest velocity in the domain is induced by the exposed electrode. Conversely, during the positive half-cycle of the excitation voltage, the largest velocity is induced by the grounded electrode, which has a negative charge. The velocity induced by the grounded electrode is smaller than that induced by the exposed electrode, because it is isolated from the fluid by the dielectric layer.

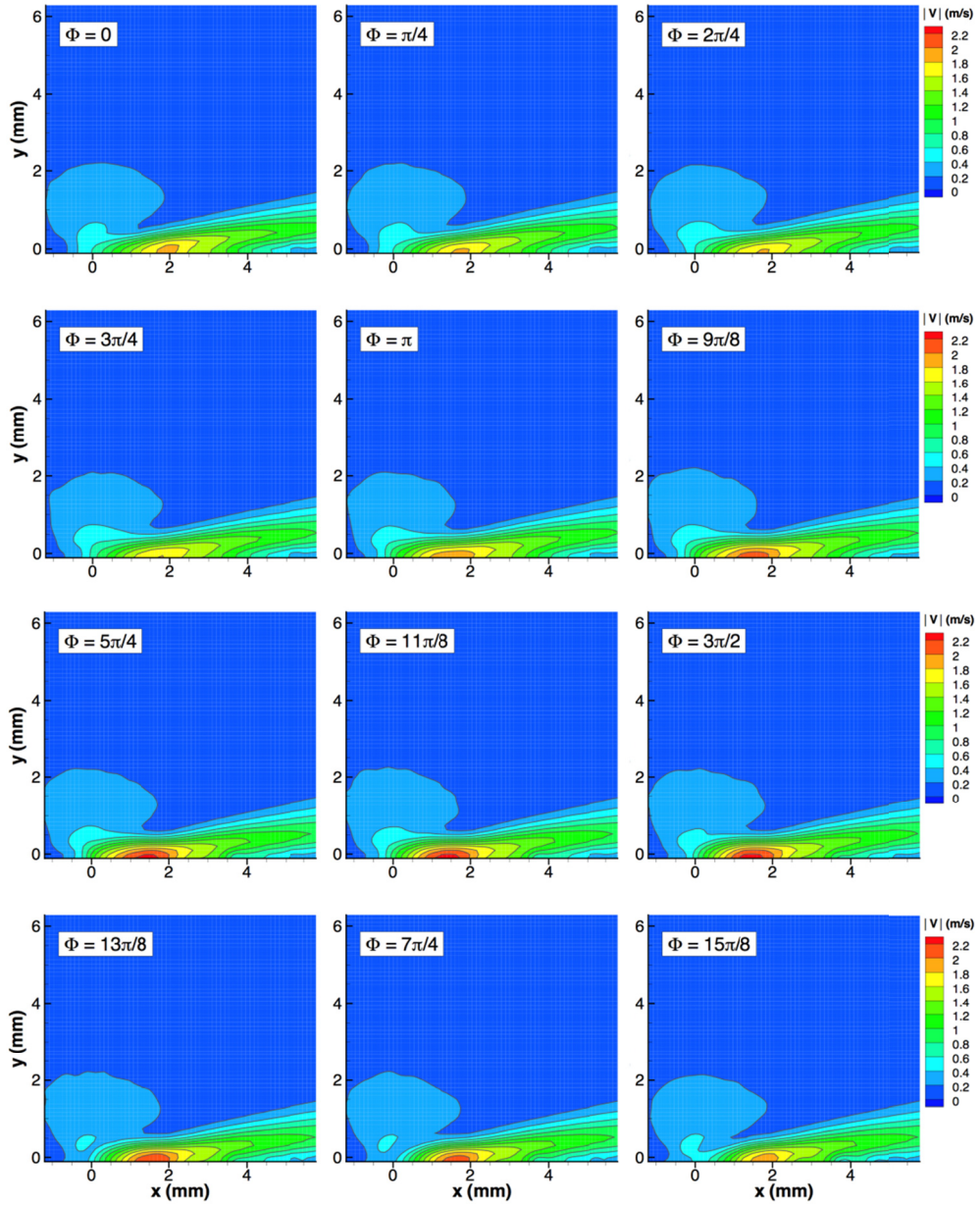

Figure 7: *Phase-averaged contours of the induced velocity magnitude* $|V| = \sqrt{u^2 + v^2}$ *for an excitation voltage of 8.8 kVpp and excitation frequency of 4 kHz.*

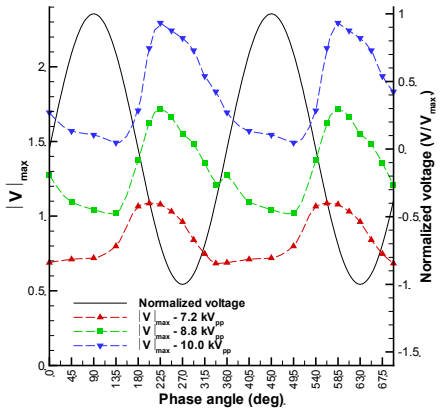

(a)

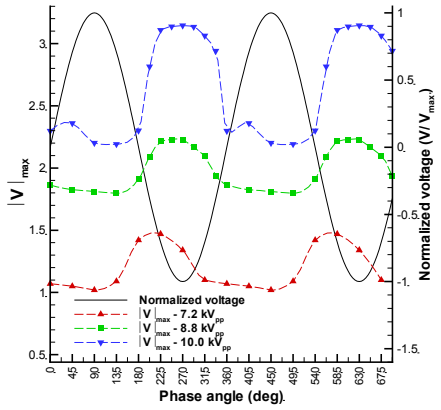

(b)

Figure 8: *Phase-averaged values of the maximum magnitude of the induced velocity* $|V|_{\max}$ *for three excitation voltages applied at (a) 2.5 kHz and (b) 4 kHz.*

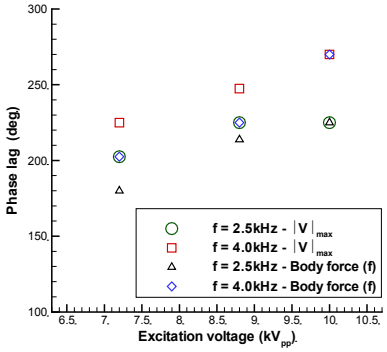

Figure 9: *Phase lag between the maxima of the induced velocity magnitude (*$|V|$*) and body force (f), and the excitation voltage.*

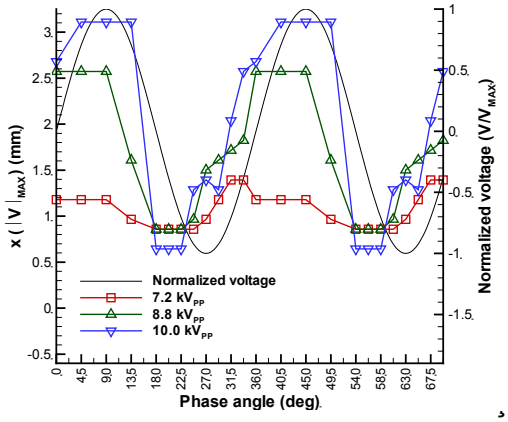

(a)

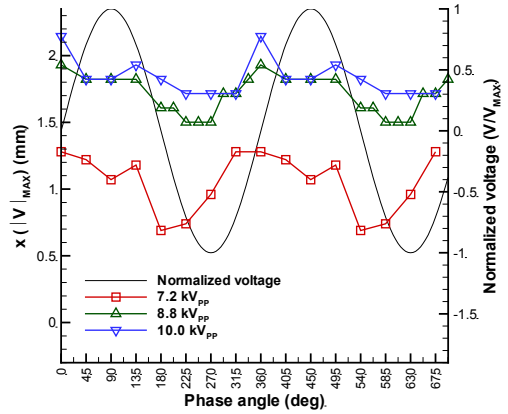

(b)

Figure 10: *Phase-dependent variations of the location of the maximum magnitude of the induced velocity* $x(|V|_{\max})$ *for three excitation voltages applied at (a) 2.5 kHz and (b) 4 kHz.*

As mentioned in the introduction one of the primary objectives of the present research is to investigate the time dependent behaviour of the velocity field around the plasma actuator with a temporal resolution comparable to that of TR-PIV measurements, through phase-locked measurements and without using costly TR-PIV apparatus. This objective can be achieved by reducing the phase interval ($\Delta\Phi$) in phase locked measurements. However, the extent to which $\Delta\Phi$ can be reduced is limited by the time interval between the two frames in a PIV snapshot. Ideally, this limit can be expressed by the following condition:

$$\frac{\Delta\Phi}{2\pi f} > \Delta t \qquad (1)$$

In Equation (1), f is the plasma actuator excitation frequency, and Δt is the time interval between the two frames in the PIV snapshot. When the phase interval so small that this condition is not met, the second frame in the PIV snapshot will no longer be captured within the intended phase interval, and therefore the phase-locked measurement will not be representative of the flow state in intended phase interval.

The approach used to overcome this limit in the present study is to improve the spatial resolution by increasing the magnification of the PIV camera, using the Questar catadioptric lens described in Section 2. Magnifying the image makes it possible to use a smaller Δt to maintain the pixel displacement consistent with the size of the interrogation window. This approach made it possible to carry out phase-locked measurements in 24 phase intervals in selected combination(s) of the excitation parameters, including excitation voltages of 8.8 kVpp and 10.0 kVpp, applied at an excitation frequency of 2.5 kHz.

Figure 11 and Figure 12 show contours of the maximum magnitude of the induced velocity in the 8.1 mm x 6.1 mm domain, for the excitation voltage of 8.8 kVpp and excitation frequency of 2.5 kHz. The figure shows the development of a high velocity region in the vicinity of the downstream edge of the exposed electrode, which reaches its maximum velocity at $\Phi = 5\pi / 4$. The high velocity region then shifts downstream over the grounded electrode.

The variation of the maximum magnitude of the induced velocity throughout the excitation cycle is shown in Figure 13, in comparison with the results of the measurements in the 31.5 mm x 15 mm domain for the same excitation parameters. The figure indicates that while the trend of variation in both experiments is similar, the velocity magnitudes measured in the 8.1 mm x 6.1 mm domain are up to 30% larger than those measured in the 31.5 mm x 15 mm domain.

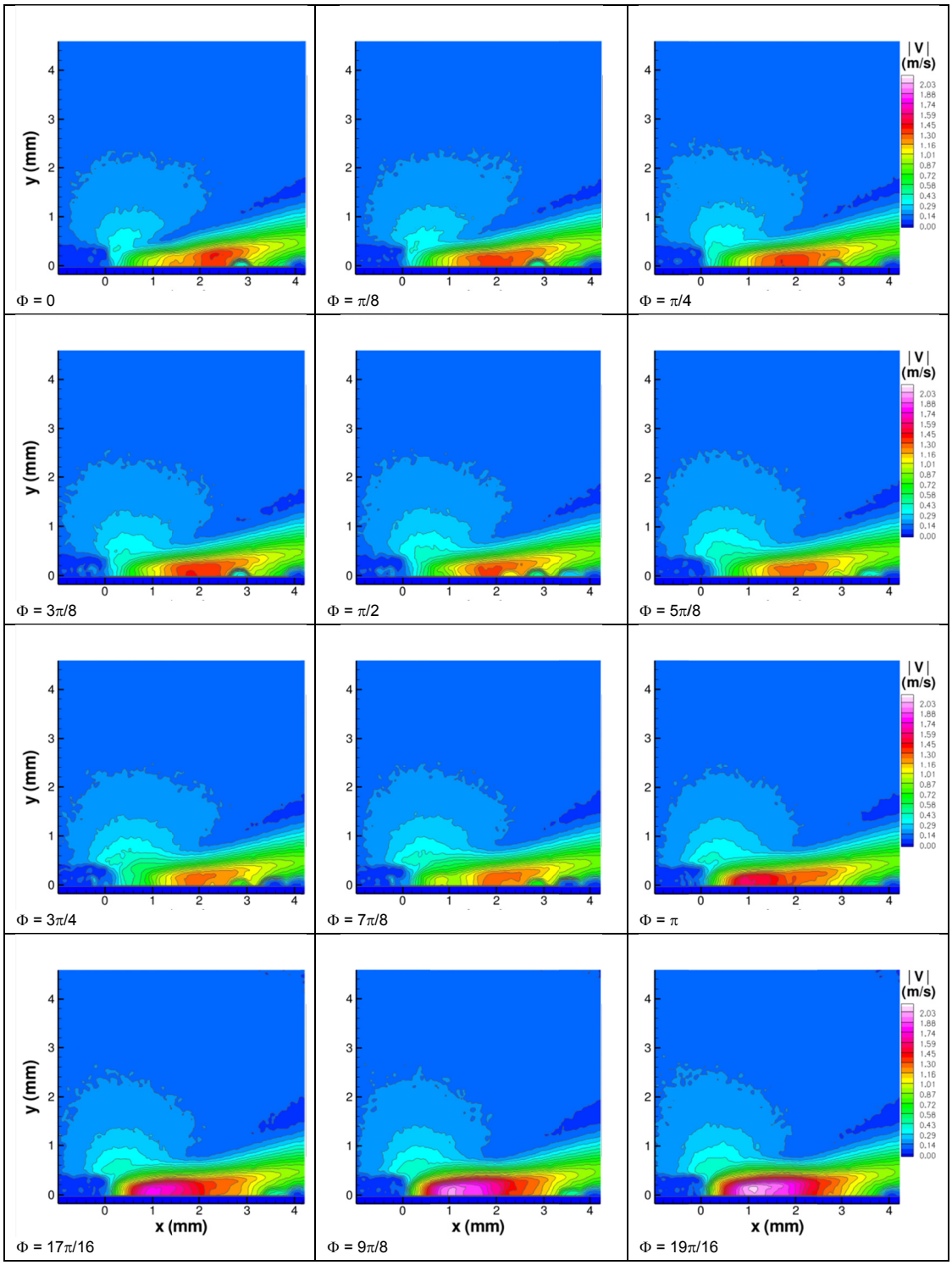

Figure 11: *Phase-averaged contours of the induced velocity magnitude* $|V| = \sqrt{u^2 + v^2}$ *for an excitation voltage of 8.8 kVpp and excitation frequency of 2.5 kHz, measured at smaller phase intervals using the Questar QM-1 microscopic lens.*

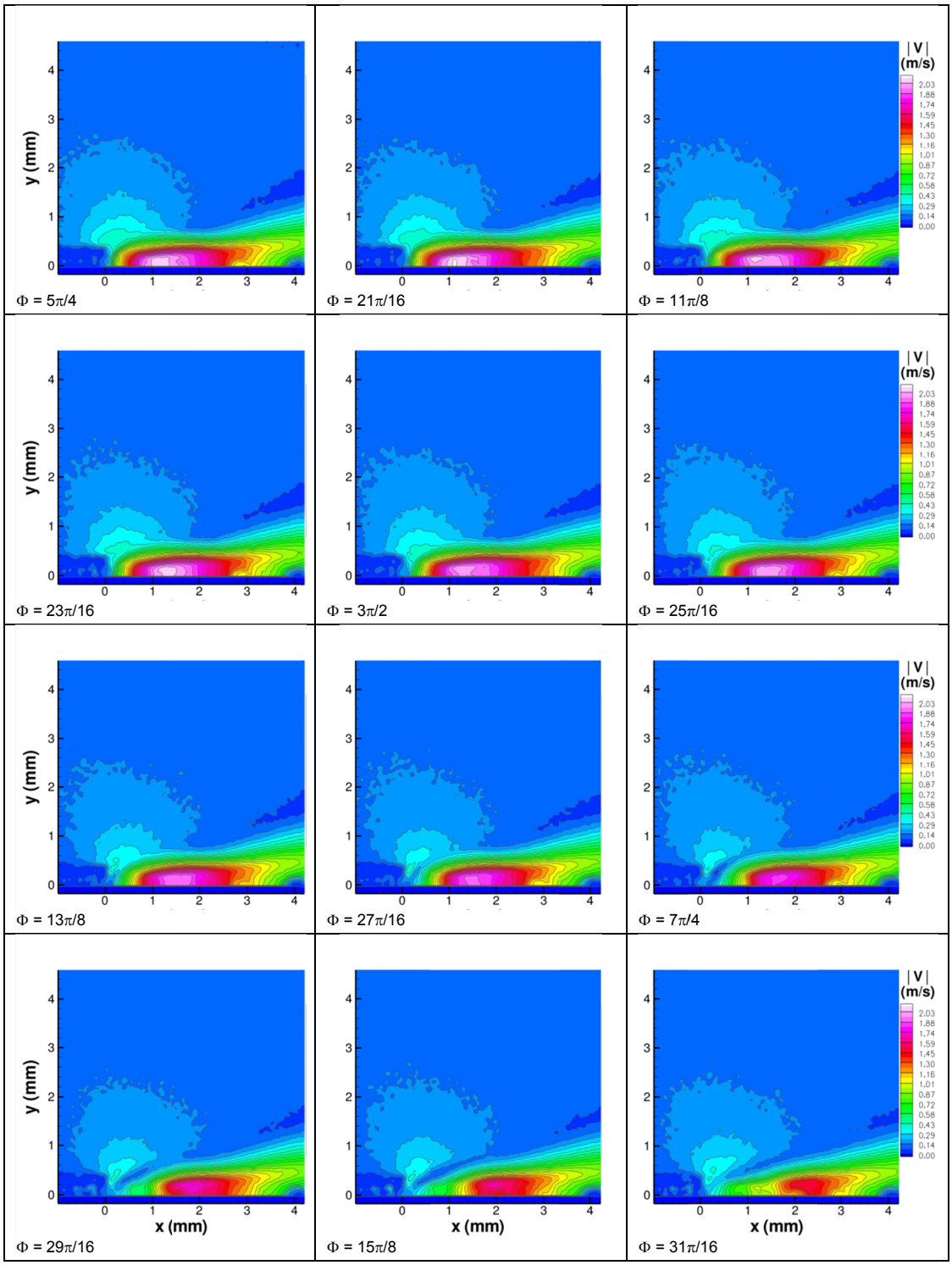

Figure 12: *Phase-averaged contours of the induced velocity magnitude* $|V| = \sqrt{u^2 + v^2}$ *for an excitation voltage of 8.8 kVpp and excitation frequency of 2.5 kHz, measured at smaller phase intervals using the Questar QM-1 microscopic lens (continued).*

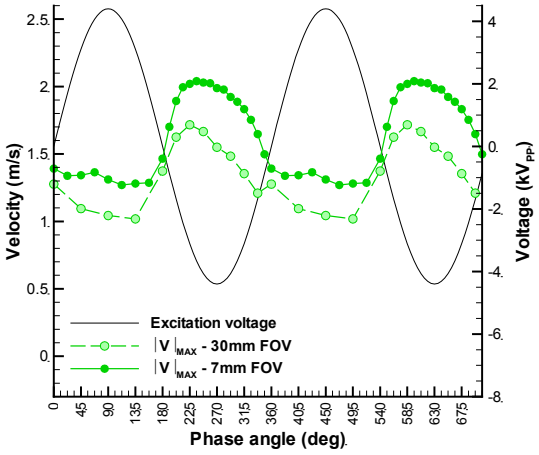

(a)

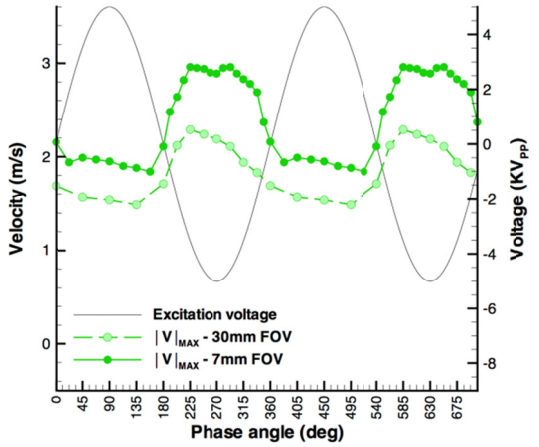

(b)

Figure 13: *Comparison of the phase-averaged values of the maximum magnitude of the induced velocity* $|V|_{\max}$ *obtained in the large and small fields of view, for excitation voltages of (a) 8.8 kVpp and (b) 10 kVpp, applied at 2.5 kHz.*

An investigation of the near-wall profiles of the induced streamwise velocity (u) in the two measurement domains helps to explain this difference. Figure 14 compares the velocity profiles obtained using the two measurement domains for the experiment at the excitation voltage of 8.8 kVpp and excitation frequency of 2.5 kHz.

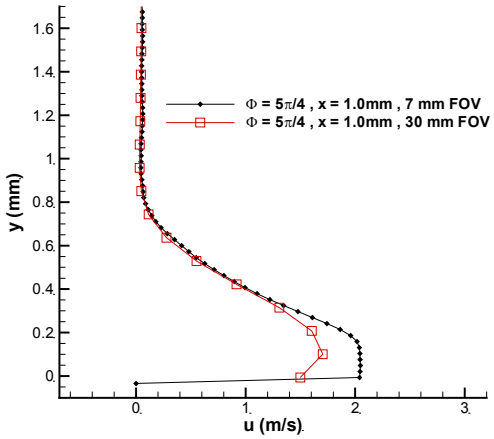

(a)

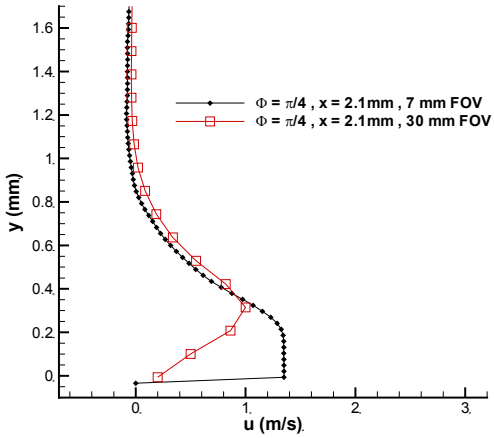

(b)

Figure 14: *Comparison of the phase-averaged velocity profiles corresponding to (a) the maximum and (b) the minimum magnitude of the induced velocity* $|V|$ *obtained in the large and small fields of view, for an excitation voltages of 8.8 kVpp applied at 2.5 kHz.*

The profiles are compared for the highest induced velocity throughout the excitation cycle, which occurs at $\Phi = 5\pi/4$ (Figure 14a), and the lowest induced velocity, which occurs at (Figure 14b). It can be observed that while the velocity profiles measured in the two domains match closely down to a distance of 0.3 mm for the wall, the maximum velocity measured in 8.1 mm x 6.1 mm domain is larger in both cases. This is because the maximum velocity occurs in a small interval in the wall normal direction, therefore, it is captured more accurately by the smaller interrogation windows of the 8.1 mm x 6.1 mm domain. On the other hand, in the 31.5 mm x 15 mm domain, the behaviour of the velocity profile below the location of the maximum velocity is more similar to that of a laminar wall jet [12], compared to that of the velocity profile in the 8.1 mm x 6.1 mm domain. This difference can be attributed to the reduced

particle density in the near wall region. Because of the reduced particle density, the smaller interrogation windows of the 8.1 mm x 6.1 mm domain are less likely to contain sufficient particles to yield a reliable value for pixel displacement, and fail to generate a realistic value for the streamwise velocity.

The phase-dependent behaviour of the location of the maximum induced velocity magnitude obtained from the measurements in the 8.1 mm x 6.1 mm domain is shown in Figure 15, in comparison with those obtained from the measurements in the 31.5 mm x 15 mm domain for similar excitation parameters.

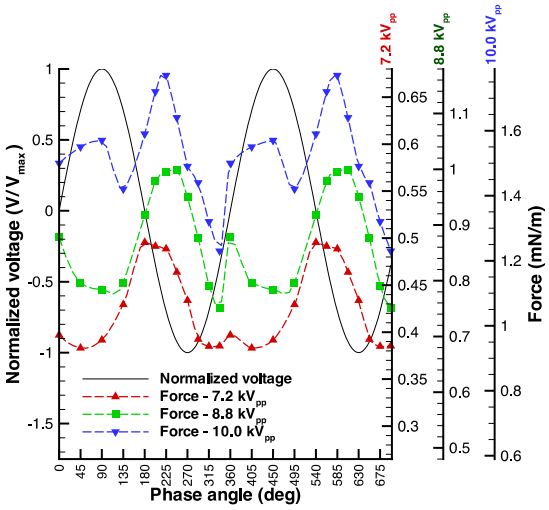

(a)

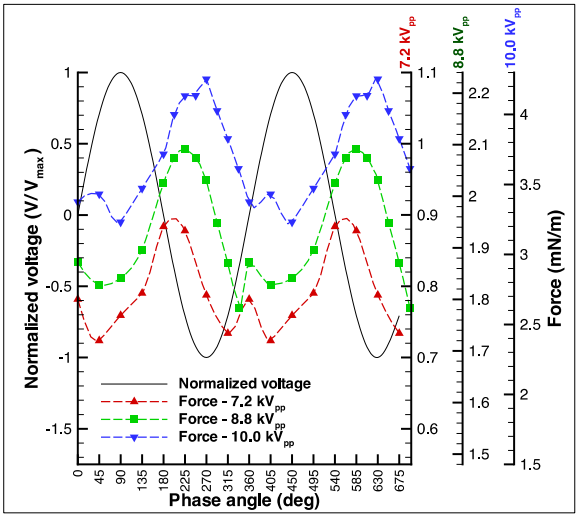

(b)

Figure 15: *Phase-averaged values of the induced body force for three excitation voltages applied at (a) 2.5 kHz and (b) 4.0 KHz.*

The figure indicates a similar behaviour for the data obtained in the two measurement domains, in which the location of the maximum induced velocity magnitude s closer to the downstream edge of the exposed electrode during the negative half of the excitation cycle, and farther from it during the positive half. In both experiments, the results obtained from measurements in the 8.1 mm x 6.1 mm domain show more scatter compared to those obtained in the 31.5 mm x 15 mm domain, because of the higher spatial resolution of the former.

In comparison, the results obtained from the 31.5 mm x 15 mm domain appear to be locked into the discrete locations of the grid points, due to the relatively large size of the interrogation windows.

3.2 The body force

The results of the phase-locked measurements of the velocity field around the plasma actuator can be used to estimate the body force generated by the actuator, based on the balance of momentum in a control volume surrounding the actuator (shown schematically in Figure 4). This method, which has been developed by Versailles et al. [10], assumes a steady, incompressible flow with constant and uniform pressure on the boundaries of the control volume. The formulation for this method can be summarized by the following equation:

$$f = \rho\int_{ab} u^2 \mathrm{d}y + \rho\int_{bc} uv\mathrm{d}x - \rho\int_{cd} u^2 \mathrm{d}y + \int_{ad} \mu\left(\mathrm{d}u/\mathrm{d}y\right)_{\mathrm{Wall}} \mathrm{d}x \qquad (2)$$

In Equation (2), f is the body force generated by the actuator in the horizontal (x) direction. The last term in Equation (2) represents the shear force generated on the wall (along the boundary *ad* in Figure 4). The effect of the location of the boundaries on the estimated body force has been investigated in the study by Murphy et al. [11] for a similar actuator. In accordance with the findings reported in [11], the boundaries *ab* and *cd* have been placed at $x = -2$ mm and $x = 15$ mm, respectively, and the boundary *bc* has been placed at $y = 15$ mm for the present calculations.

Figure 16 shows the phase-dependent behaviour of the estimated body force for three excitation voltages (7.2 kVpp, 8.8 kVpp, and 10 kVpp), applied at excitation frequencies of 2.5 kHz and 4.0 kHz, respectively. The behaviour of the body force is generally similar to that of the induced velocity, as discussed in Section 3.1. The primary peak in the body force corresponds to the maximum induced velocity, as they both appear at the same phase angle during the negative half-cycle of the excitation signal. Similarly, a phase lag exists between the maximum body force and the peak excitation voltage, which increases slightly when the actuator is excited with a higher voltage, as shown in Figure 9. This effect is more pronounced at the excitation frequency of 4 kHz, where relatively larger values of phase lag are observed.

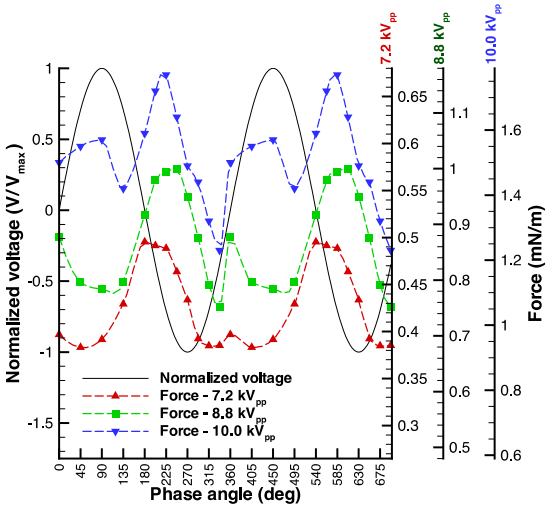

(a)

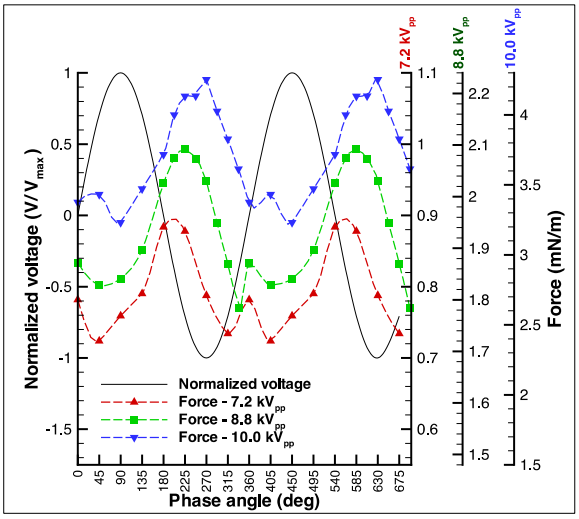

(b)

Figure 16: *Phase-averaged values of the induced body force for three excitation voltages applied at (a) 2.5 kHz and (b) 4.0 KHz.*

Figure 16 also shows a smaller secondary peak in the phase-dependent variations of the body force, at the approximate phase angle of $\Phi = 2\pi$. An investigation of the time-dependent variation of the electric current passing through the plasma actuator, shown in Figure 17 for an excitation voltage of 8.8 kVpp and frequency of 4.0 kHz, indicates that the phase angle of this secondary peak corresponds with spikes the positive electric current, which are believed to be caused by small and localized discharges associated with formation of the plasma near the grounded electrode during the positive half cycle of the excitation signal [6]. The phase-dependent behaviour of the location of the maximum induced velocity magnitude (Figure 10) supports this hypothesis, because it shows that during the positive half of the excitation signal, the location of the maximum induced velocity shifts downstream towards the grounded electrode.

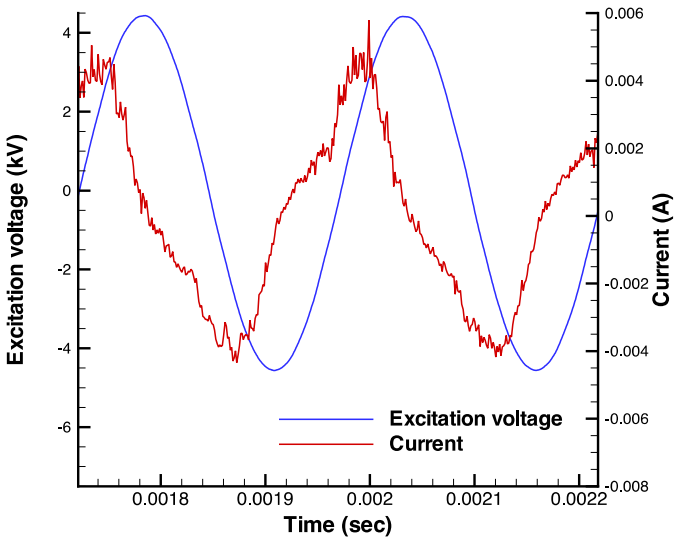

Figure 17: *A sample of the time series of the excitation voltage and current from the experiment at 8.8 kVpp and 4 KHz, showing the current spikes.*

Kotsonis and Ghaemi [6] have reported a similar correspondence between the spikes in the positive electric current and a secondary peak in the local fluid acceleration induced by the plasma actuator through the positive half cycle of the excitation signal, based on time-resolve PIV measurements of the velocity field. While the observation by Kotsonis and Ghaemi [6] is limited to a single point in the flow field, the results of the present study indicate that the effects of the formation of plasma near the grounded electrode during the positive half cycle of the excitation signal is more widespread, as indicated by the secondary peak in the body force.

The ratio of the magnitude of the secondary peak of the body force to the primary peak is shown in Figure 18, for the excitation voltages and frequencies investigated in the present study. The figure indicates that the relative magnitude of the secondary peak grows as excitation voltage and frequency increase. Considering the fact that the secondary peak is associated with the formation of plasma over the grounded electrode during the positive half cycle of the excitation signal, this behaviour indicates that the effectiveness of the dielectric layer in isolating the grounded electrode from the fluid decreases at higher excitation voltages and frequencies.

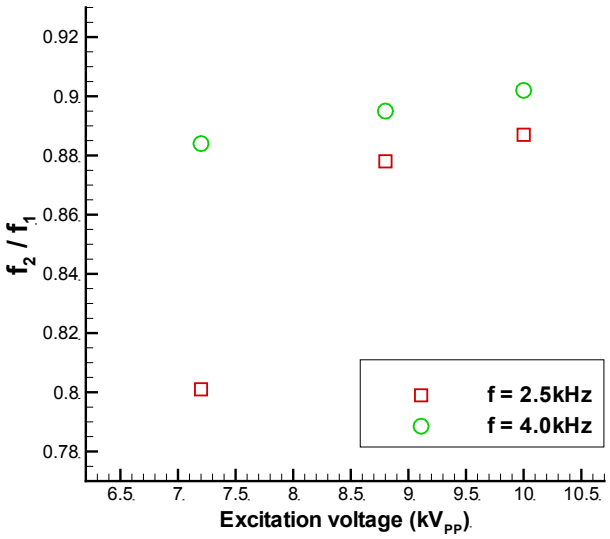

Figure 18: *The ratio of the magnitude of the secondary peak (f2) of the body force to the primary peak (f1).*

Murphy et al. [11] have shown that the wall shear stress, represented by the last term in Equation (2), constitutes up to 30% of the body force. Considering the significance of this term, the role of the estimation method for the wall-normal derivative in the shear stress term has been investigated in the present study. In previous studies ([8], [11]) this term has been estimated using the following first order numerical derivation scheme

$$\left(\frac{\mathrm{d}u}{\mathrm{d}y}\right)_{\mathrm{wall}} = \frac{u_{\mathrm{l}}}{\Delta y} \tag{3}$$

in which is the horizontal velocity component at the first measurement point above the boundary *ad*, and Δy is the distance of the measurement point from the boundary. This method is evidently dependent on the spatial resolution of the measurement technique in the wall-normal direction, as well as the accuracy of the velocity measured adjacent to the wall, which is usually affected by reflections from the wall and reduced particle density.

The other approach for estimating the wall normal derivative is based on the assumption that the plasma actuator generates a two-dimensional laminar wall jet. Glauert [12] has shown that the self-similar velocity profile in a two-dimensional wall jet ($f'(\eta)$) is given by the solution of the following ordinary differential equation

$$f''' + ff'' + 2f'^2 = 0 \tag{4}$$

with boundary conditions $f(0) = f'(0) = 0$ and $f'(\infty) = 0$. The term $\left(\frac{du}{dy}\right)_{wall}$ is then estimated by scaling the derivative of the self-similar velocity profile, using

$$\left(\frac{du}{dy}\right)_{wall} = \left(\frac{u_{max}}{f'_{max}}\right)\left(\frac{\eta_{max}}{y_{max}}\right)\left(\frac{df'}{d\eta}\right)_{wall} . \quad (5)$$

Numerical solution of Equation (4) yields the following values for the terms in Equation (5).

$$\left(\frac{df'}{d\eta}\right)_{wall} = 0.2222 , \; f'_{max} = 0.3150 , \text{ and } \eta_{max} = 2.0287 .$$

Equation (5) is therefore simplified to

$$\left(\frac{du}{dy}\right)_{wall} = 1.4310\frac{u_{max}}{y_{max}} \quad (6)$$

in which u_{max} is the local maximum velocity of the wall jet at any given streamwise (x) location, and y_{max} is the location of the maximum velocity in the wall-normal direction. Rather than relying on the velocity adjacent to the wall, this method relies on the maximum velocity of the wall jet, which usually occurs away from the wall. Therefore, it is expected to be less sensitive to spatial resolution of the PIV measurements and less likely to be affected by the quality of velocity measurement adjacent to the wall.

The results of estimation of the body force using the two above-mentioned methods to estimate the wall-normal derivative in the shear stress term are compared in Figure 19 for the excitation frequency of 2.5 kHz and excitation voltages of 8.8 kVpp and 10.0 kVpp. The figures show the results obtained in both the 31.5 mm x 15 mm and the 8.1 mm x 6.1 mm measurement domains. It can be observed that there is a difference of up to 30% between the values of the body force obtained using the two methods in the 31.5 mm x 15 mm domain. However, the results of the two methods match very closely in the 8.1 mm x 6.1 mm domain, with a maximum difference no more than 6%. The close match between the results of the two methods in the 8.1 mm x 6.1 mm domain can be attributed to the improved spatial resolution in that domain, which makes it possible to determine u_1, u_{max}, and y_{max} more accurately.

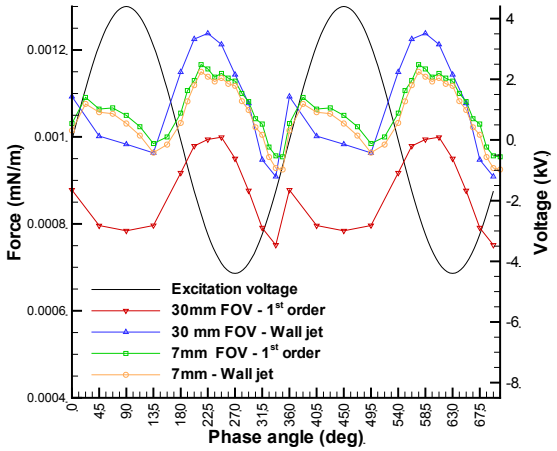

(a)

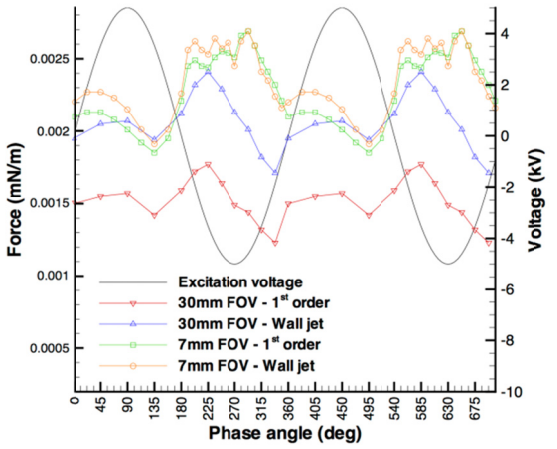

(b)

Figure 19: *The effect of the method of estimation of* $\frac{du}{dy}$ *at the boundary ad of the flow control volume on the estimated body force for excitation voltages of (a) 8.8 kVpp and (b) 10 kVpp applied at 2.5 kHz.*

3.3 Direct force measurements

In order to evaluate the results of the estimation of the body force based on PIV measurements, direct measurements of the force generated by the actuator were carried out, as described in Section 2. According to the study by Hoskinson et al. [13], when the shear force acting on the surface due to the flow induced by the actuator is small compared to the force due to the momentum induced by the actuator, the force measured by the balance will be close to the momentum component of the force generated by the actuator, which is represented by the first

three terms of Equation (2). However, as shown by the results of the present study, as well as the study by Murphy et al. [11], the shear force comprises a significant part of the actuator body force for the present plasma actuator configuration, and is not negligible. Therefore, as shown by Ashpis et al. [14], the force measured directly by the balance is expected to include the effect of the shear force, which is represented by the last term in Equation (2).

The results of the direct force measurements are compared to the forces obtained based on the PIV measurements using the control volume method (Section 3.2), in Figure 20. Each of the data points representing direct force measurements are based on three independent measurements.

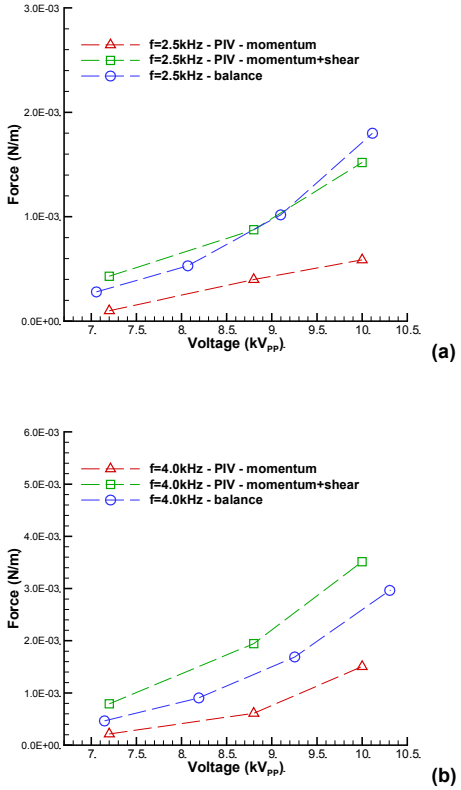

Figure 20: *Comparison of the results of the direct force measurements to the forces obtained based on PIV measurements using the control volume method at (a) f = 2.5 kHz and (b) f = 4 kHz.*

It can be observed that in all combinations of excitation voltage and frequency, the results of the direct force measurements are larger than the momentum-based component of the force, estimated using the first three terms of Equation (2), and that at the excitation frequency of $f = 2.5\,\mathrm{kHz}$, they are close to the estimated total force, which includes the shear force component. This observation confirms that the shear force component is indeed a significant contributor to the total body force in the present plasma actuator configuration. However, the difference between the results of direct force measurements and the estimated total force at $f = 4.0\,\mathrm{kHz}$ suggests that further improvement in the methodology for estimating the shear force component may be needed.

4 Conclusions and recommendations

In the present study, phase-locked PIV measurements have been carried out using a conventional PIV system, to investigate the time-dependent behaviour of plasma actuators with a temporal resolution comparable to those achieved in previous studies using TR-PIV. The phase-locked measurement technique has been found to be advantageous over TR-PIV, because it allows measurement of the time-dependent behaviour of plasma actuators excited at relatively high frequencies (up to 4 KHz in the present experiments), without requiring high-speed cameras and laser light sources. The present technique also does not suffer from decreased camera resolution associated with high-speed cameras operated at high capture rates, and can therefore provide results with more adequate spatial resolution. In the present experiments, vector spacings of 0.1 mm and 0.03 mm have been achieved in domains measuring 31.5 mm x 15 mm and 8.1 mm x 6.1 mm, respectively. Measurements have been carried out in up to 24 phase intervals throughout the excitation signal, which is applied at frequencies of 2.5 kHz and 4.0 kHz. To achieve a similar temporal resolution, a TR-PIV system would require a sampling frequency up to 96 kHz, which is beyond the capability of commercially available systems.

The results of the present measurements indicate that a phase lag exists between the maximum induced velocity by the plasma actuator and the excitation signal. A similar phase lag also exists between the body force induced by the actuator and the excitation signal. The phase lag is found to have values between 180° and 270°, depending on the excitation voltage and frequency. In general, the phase lag increases when the excitation voltage or frequency are increased. Characterization of the phase lag, carried out in the present study, is significant from the point of view of application of plasma actuators in active flow control, especially when the characteristic time scales of the flow phenomena are close to those of the plasma actuator.

The phase-dependent behaviour of the body force, estimated using a control volume method based on the results of the PIV measurements, shows a secondary peak. While the maximum induced body force throughout the excitation cycle is concurrent with the negative half-cycle of the excitation signal, the secondary peak occurs during the positive half-cycle of the excitation signal. The magnitude of the secondary peak, which varies between 80% and 90% of the maximum induced body force, is found to be dependent on the excitation voltage and frequency. In general, the magnitude of the secondary peak increases when the excitation voltage or frequency are increased.

The results of the phase-locked velocity field measurements in the 8.1 mm x 6.1 mm domain, which have been carried out at 24 phase intervals, indicated that the secondary peak is due to the formation of a secondary high-velocity region near the grounded electrode during the positive half-cycle of the excitation signal. The formation of this secondary high-velocity region has been observed in the results of the TR-PIV measurements reported by Kotsonis and Ghaemi [6], and attributed to small and localized discharges associated with formation of the plasma near the grounded electrode during the positive half-cycle of the excitation signal. The spikes of the electric current observed in the present experiments during the positive half-cycle of the excitation signal support this hypothesis. Furthermore, the trend of variation of the magnitude of secondary peak indicates that the effectiveness of the dielectric layer in isolating the grounded electrode from the fluid decreases at higher excitation voltages and frequencies.

The results of the estimation of the induced body force using the control volume method indicated that the shear force acting on the surface of the actuator due to the induced flow is a significant contributor to the total body force. Since the shear force is proportional to the value of the wall-normal derivative of streamwise velocity at the surface of the actuator in the formulation of the control volume method, two different methods for estimating the wall-normal derivative have been evaluated. In one method, the derivative is calculated numerically based on the results of the PIV measurements. The other method is based on the assumption that the velocity induced by the actuator is represented by a laminar wall jet, and uses the self-similar solution of the laminar wall-jet problem to determine the derivative. Comparison of the results of the two methods indicates a difference of up to 30% in the body force estimated based on the measurements in the 31.5 mm x 15 mm domain. However, when the measurements in the 8.1 mm x 6.1 mm domain are used to estimate the body force, the difference between the results of the two methods is limited to 6%. The convergence of the results of the two methods in the 8.1 mm x 6.1 mm domain can be attributed to the higher spatial resolution, which makes it possible to measure the maximum induced velocity in the near wall region more accurately.

In order to evaluate the results of the estimation of the body force base on the PIV measurements, direct force measurements have been carried out using a precision balance. The results indicate that in all combinations of excitation voltage and frequency, the body force measured by the balance is larger than the momentum-based component of the body force estimated using the PIV results. At the excitation frequency of f = 2.5 kHz, the PIV-based body forces are close to those obtained from direct balance measurements. At f = 4 kHz, however, the control volume method over-estimates the body force.

Based on the findings summarized above, the following recommendations can be made to expand the scope and improve the results of the present study:

The PIV measurements have been carried out in a relatively limited range of excitation parameters, which includes three voltages and two frequencies. It is therefore recommended to expand this range, to ensure that the observed findings and trends remain valid for a more comprehensive set of excitation parameters.

Furthermore, a more limited range of excitation parameters (including two voltages and one frequency) has been selected for a more detailed study with higher spatial and temporal resolution. Considering the differences observed between the results of the detailed study and the original PIV experiments, it is recommended carry out the detailed measurements with improved spatial and temporal resolution for more combinations of the excitation parameters, to examine the consistency of the differences observed between the two sets of results.

Considering the fact that the body force estimated based on the PIV measurements is sensitive to the estimated wall-normal derivative of the streamwise velocity at the surface of the actuator, it is recommended to explore measures to improve the quality of measurement in the near-wall region. These measures may include alternative seeding techniques and materials to improve the particle density in the near-wall region.

While values of body force estimated using the PIV results are close to those obtained through direct force measurements at f = 2.5 kHz, the PIV-based estimation method over-estimates the body force at f = 4.0 kHz, in comparison to the values obtained from the direct measurements. It is therefore recommended to further improvement the method, and in particular the estimation of the shear force.

This page intentionally left blank.

References

[1] R. Hanson, P. Lavoie, A. Naguib, and J. Morrison, “Transient growth instability cancellation by a plasma actuator array”, Experiments in Fluids, vol. 49, pp. 1339–1348, (2010).

[2] T. Jukes, T. Segawa, and H. Furutani, “Active flow separation control on a NACA 4418 airfoil using DBD vortex generators and FBG sensors”, in 50th AIAA Aerospace Sciences Meeting, no. AIAA 2012-1193, (Nashville, Tennessee, USA), (2012).

[3] Z. Kozlov, and F. Thomas, “Bluff-body flow control via two types of dielectric barrier discharge plasma actuation”, AIAA Journal, vol. 49, no. 9, pp. 1919–1931, (2011).

[4] V. Boucinha, R. Joussot, P. Magnier, R. Weber, and A. Leroy-Chesneau, “Characterization of the ionic wind produced by a dbd actuator designed to control the laminar-to-turbulent transition”, in Proceedings of the 14th International Symposium on Application of Laser Techniques to Fluid Mechanics, no. 1352, (Lisbon, Portugal), (2008).

[5] N. Houser, “Manufacturing of dielectric barrier discharge plasma actuators for degredation resistance”, M.A.Sc. Thesis, University of Toronto Institute for Aerospace Studies, Toronto, Ontario, Canada, (2013).

[6] M. Kotsonis, and S. Ghaemi, “Performance improvement of plasma actuators using asymmetric high voltage waveforms”, Journal of Physics D: Applied Physics, vol. 45, no. 4, p. 045204, (2012).

[7] W. Kim, H. Do, M. G. Mungal, and M. A. Cappelli, “On the role of oxygen in dielectric barrier discharge actuation of aerodynamic flows”, Applied Physics Letters, vol. 91, pp. 181501-1-3, (2007).

[8] J. Murphy, J. Kriegseis, and P. Lavoie, “Scaling of maximum velocity, body force, and power consumption of dielectric barrier discharge plasma actuators via particle image velocimetry”, Journal of Applied Physics, vol. 133, pp. 243301-1-10, (2013).

[9] J. Kriegseis, B. Moller, S. Grundmann, and C. Tropea, “Capacitance and power consumption quantification of DBD plasma actuators”, Journal of Electrostatics, vol. 69, pp. 302–312, (2011).

[10] P. Versailles, V. Gingras-Gosselin, and H. D. Vo, “Impact of pressure and temperature on the performance of plasma actuators," AIAA Journal, vol. 48, pp. 859–863, (2010).

[11] J. Murphy, and P. Lavoie, “Characterization of DBD plasma actuators via PIV measurements”, in 51st AIAA Aerospace Sciences Meeting, no. AIAA 2013-0346, (Grapevine, Texas, USA), (2013).

[12] M. B. Glauert, “The wall jet”, Journal of Fluid Mechanics, vol. 1, no. 6, pp. 625–643, (1956).

[13] R. Hoskinson, N. Hershkowitz, and D. E. Ashpis, “Force measurements of single and double barrier DBD plasma actuators in quiescent air”, Journal of Physics D: Applied Physics, vol. 41, no. 24, p. 245209, (2008).

[14] D. E. Ashpis, and M. C. Laun, “Dielectric barrier discharge plasma actuator thrust — Measurement methodology incorporating new anti-thrust hypothesis”, in 52nd AIAA Aerospace Sciences Meeting, no. AIAA 2014-0486, (National Harbor, Maryland, USA), (2014).

List of symbols/abbreviations/acronyms/initialisms

AC	Alternating Current
AWG	American wire gauge
CCD	Charge-Coupled Device
DBD	Dielectric Barrier Discharge
DND	Department of National Defence
DRDC	Defence Research and Development Canada
DSTKIM	Director Science and Technology Knowledge and Information Management
EHD	Electrohydrodynamic
LDV	Laser Doppler Velocimetry
MDN	Ministère de la défense nationale
PIV	Particle Image Velocimetry
PMMA	Poly(methyl-methacrylate)
R&D	Research & Development
TR-PIV	Time-Resolved Particle Image Velocimetry

This page intentionally left blank.

DOCUMENT CONTROL DATA

(Security markings for the title, abstract and indexing annotation must be entered when the document is Classified or Designated)

1. ORIGINATOR (The name and address of the organization preparing the document. Organizations for whom the document was prepared, e.g., Centre sponsoring a contractor's report, or tasking agency, are entered in Section 8.)

Defence Research and Development Canada – Valcartier
2459 Pie-XI Blvd North
Quebec (Quebec)
G3J 1X5 Canada

2a. SECURITY MARKING (Overall security marking of the document including special supplemental markings if applicable.)

UNCLASSIFIED

2b. CONTROLLED GOODS

(NON-CONTROLLED GOODS)
DMC A
REVIEW: GCEC DECEMBER 2012

3. TITLE (The complete document title as indicated on the title page. Its classification should be indicated by the appropriate abbreviation (S, C or U) in parentheses after the title.)

Force measurements on plasma actuators using phase-locked particle image velocimetry

4. AUTHORS (last name, followed by initials – ranks, titles, etc., not to be used)

Pimentel, R.; Lahouti, A.; Lavoie, P.

5. DATE OF PUBLICATION (Month and year of publication of document.)	6a. NO. OF PAGES (Total containing information, including Annexes, Appendices, etc.)	6b. NO. OF REFS (Total cited in document.)
May 2015	36	14

7. DESCRIPTIVE NOTES (The category of the document, e.g., technical report, technical note or memorandum. If appropriate, enter the type of report, e.g., interim, progress, summary, annual or final. Give the inclusive dates when a specific reporting period is covered.)

Scientific Report

8. SPONSORING ACTIVITY (The name of the department project office or laboratory sponsoring the research and development – include address.)

Defence Research and Development Canada – Valcartier
2459 Pie-XI Blvd North
Quebec (Quebec)
G3J 1X5 Canada

9a. PROJECT OR GRANT NO. (If appropriate, the applicable research and development project or grant number under which the document was written. Please specify whether project or grant.)	9b. CONTRACT NO. (If appropriate, the applicable number under which the document was written.)

10a. ORIGINATOR'S DOCUMENT NUMBER (The official document number by which the document is identified by the originating activity. This number must be unique to this document.)	10b. OTHER DOCUMENT NO(s). (Any other numbers which may be assigned this document either by the originator or by the sponsor.)
DRDC-RDDC-2015-R071	

11. DOCUMENT AVAILABILITY (Any limitations on further dissemination of the document, other than those imposed by security classification.)

Unlimited

12. DOCUMENT ANNOUNCEMENT (Any limitation to the bibliographic announcement of this document. This will normally correspond to the Document Availability (11). However, where further distribution (beyond the audience specified in (11) is possible, a wider announcement audience may be selected.))

Unlimited

13. ABSTRACT (A brief and factual summary of the document. It may also appear elsewhere in the body of the document itself. It is highly desirable that the abstract of classified documents be unclassified. Each paragraph of the abstract shall begin with an indication of the security classification of the information in the paragraph (unless the document itself is unclassified) represented as (S), (C), (R), or (U). It is not necessary to include here abstracts in both official languages unless the text is bilingual.)

Phase-locked Particle Image Velocimetry (PIV) has been used to investigate the time-dependent behaviour of a Dielectric Barrier Discharge (DBD) plasma actuator, excited by a sine-wave signal with peak-to-peak amplitudes between 7.2 kV and 10 kV, and frequencies of 2.5 kHz and 4 kHz. Measurements were initially carried out in a 31.5 mm x 15 mm domain, resulting in a spatial resolution of 0.1072 mm, in 12 phase intervals throughout the excitation cycle. In order to improve the spatial and temporal resolution, additional measurements were carried out for a subset of the excitation parameters in an 8.1 mm x 6.1 mm domain, resulting in a spatial resolution of 0.0276 mm in 24 phase intervals. Momentum balance in a control volume surrounding the actuator has been used to estimate the body force based on the results of the PIV measurements. The results indicate that the maximum induced velocity and body force occur during the negative half-cycle of the excitation signal, with a phase lag relative to the excitation signal that grows when excitation voltage or frequency is increased. A smaller, secondary peak is observed in the induced body force, occurring during the positive half-cycle of the excitation signal. The results suggest that this peak is due to formation of a secondary high-velocity region due to local discharges near the grounded electrode. Two methods have been used to determine the shear force, resulting up to 25% variability in the estimated body force. Considering this variability, direct force measurements have been carried out using a precise balance to validate the results of the PIV-based control volume approach. The difference observed in certain conditions between the estimated body forces and those measured directly highlight the need for further improving the methodology for body force prediction based on PIV measurements.

---

14. KEYWORDS, DESCRIPTORS or IDENTIFIERS (Technically meaningful terms or short phrases that characterize a document and could be helpful in cataloguing the document. They should be selected so that no security classification is required. Identifiers, such as equipment model designation, trade name, military project code name, geographic location may also be included. If possible keywords should be selected from a published thesaurus, e.g., Thesaurus of Engineering and Scientific Terms (TEST) and that thesaurus identified. If it is not possible to select indexing terms which are Unclassified, the classification of each should be indicated as with the title.)

Plasma actuator, Dielectric Barrier Discharge, DBD, Particle Image Velocimetry, PIV, Phase-locked PIV